Highly-efficient thermoelectronic conversion of solar energy and heat into electric power

Stefan Meir, Cyril Stephanos, T. H. Geballe, Jochen Mannhart

Angaben zur Veröffentlichung / Publication details:

Meir, Stefan, Cyril Stephanos, T. H. Geballe, and Jochen Mannhart. 2013. "Highly-efficient thermoelectronic conversion of solar energy and heat into electric power." *Journal of Renewable and Sustainable Energy* 5 (4): 043127. https://doi.org/10.1063/1.4817730.

Highly-efficient thermoelectronic conversion of solar energy and heat into electric power

S. Meir, C. Stephanos, T. H. Geballe, and J. Mannhart

Citation: Journal of Renewable and Sustainable Energy **5**, 043127 (2013); doi: 10.1063/1.4817730
View online: https://doi.org/10.1063/1.4817730
View Table of Contents: http://aip.scitation.org/toc/rse/5/4
Published by the American Institute of Physics

Highly-efficient thermoelectronic conversion of solar energy and heat into electric power

S. Meir,[1,a)] C. Stephanos,[1,2,a)] T. H. Geballe,[3] and J. Mannhart[2,b)]
[1]*Experimental Physics VI, Center for Electronic Correlations and Magnetism, Augsburg University, 86135 Augsburg, Germany*
[2]*Max Planck Institute for Solid State Research, 70659 Stuttgart, Germany*
[3]*Department of Applied Physics and Laboratory for Advanced Materials, Stanford University, Stanford, California 94305-4045, USA*

(Received 5 February 2013; accepted 17 July 2013; published online 19 August 2013)

Electric power may, in principle, be generated in a highly efficient manner from heat created by focused solar irradiation, chemical combustion, or nuclear decay by means of thermionic energy conversion. As the conversion efficiency of the thermionic process tends to be degraded by electron space charges, the efficiencies of thermionic generators have amounted to only a fraction of those fundamentally possible. We show that this space-charge problem can be resolved by shaping the electric potential distribution of the converter such that the static electron space-charge clouds are transformed into an output current. Although the technical development of such thermoelectronic generators will require further substantial efforts, we conclude that a highly efficient transformation of heat to electric power may well be achieved. [http://dx.doi.org/10.1063/1.4817730]

I. INTRODUCTION

Electric power can be generated in a highly efficient manner via thermionic energy conversion from heat created by focused solar irradiation or combustion of fossil fuels.[1–4] Generators based on the thermionic process could, if implemented, considerably enhance the efficiency of focused solar energy conversion or of coal combustion power plants,[5] yielding a corresponding reduction of CO_2 emissions. In thermionic energy conversion a vacuum is applied as the active material between the electrodes, rather than the solid conductors that give rise to the thermoelectric effect.[6] Thereby, the parasitic heat conduction from the hot to the cold electrode is radically decreased.

Thermionic generators can operate with input temperatures T_{in} that are sufficiently high to match the temperatures at which concentrating-solar power plants or fossil-fuel power stations generate heat. In principle, electric power may therefore be generated from these energy sources with outstanding efficiency because the maximum possible efficiency – the Carnot efficiency $\eta_C = 1 - T_{out}/T_{in}$ – increases with T_{in}, where T_{out} is the generator's output temperature.[7] In contrast, a significant amount of energy is wasted today in the conversion of heat to electricity. Coal, from which 40 % of the world's electricity is currently generated,[8] is burned in power stations at ∼1500 °C, whereas, due to technical limitations, the steam turbines driven by this heat are operated below ∼700 °C, to give but one example.

However, thermionic generators have never been deployed to harvest solar energy or to convert combustion heat into electricity in power stations[9] or cars,[10] although the conversion process is straightforward and appears to be achievable: electrons are evaporated from a heated emitter

[a)]S. Meir and C. Stephanos contributed equally to this work.
[b)]Author to whom correspondence should be addressed. Electronic mail: j.mannhart@fkf.mpg.de

electrode into vacuum, then the electrons drift to the surface of a cooler collector electrode, where they condense.[3,6] If used for solar energy harvesting, the quantum nature of light can be exploited for great efficiency gains by using photon-enhanced thermionic emission (PETE).[4,11] PETE employs the photoeffect to enhance electron emission by lifting the electron energy in a semiconducting emitter across the bandgap D into the conduction band, from where the electrons are thermally emitted. As a result of the electron flow, the electrochemical potentials of the emitter and collector differ by a voltage $V_{\rm out}$, and an output current $I_{\rm ec} = V_{\rm out}/R_{\rm l}$ can be sourced through a load resistor $R_{\rm l}$. Turning this elegant operation principle into commercial devices has not yet been possible, however, because space-charge clouds suppress the emission current for emitter-collector distances of $d_{\rm ec} > 3 - 5\,{\rm l m}$.[6,12,13] Practical fabrication of emitter-collector assemblies that operate with the required close tolerances at a temperature difference $T_{\rm e} - T_{\rm c}$ of many hundred Kelvin was found to be highly challenging.[14] In addition, for $d_{\rm ec} < 1\,{\rm l m}$, near-field infrared thermal losses between emitter and collector become large.[15] For large $d_{\rm ec}$, it has only been possible to suppress the space charges by neutralizing them, which was done by inserting Cs^+ ions into the space-charge cloud,[16,17] a method used in two 5 kW nuclear-powered thermionic generators aboard experimental Soviet satellites.[14,18] With that approach, compensating the space charge by ion injection causes a $\sim$50 % loss of output power $P_{\rm out}$.[10] Novel schemes[10] to suppress the space charges by optimizing the generation of Cs^+ have yet to be demonstrated. Since the 1950s, when the space-charge problem was first approached,[3,6,19] it has remained the main obstacle to achieving efficient thermionic generators.[3,10]

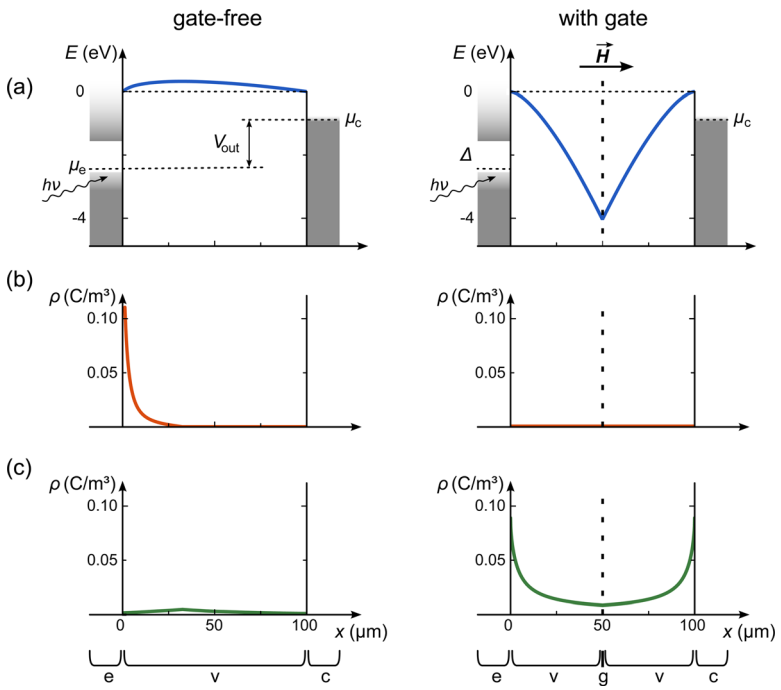

FIG. 1. Sketch of the working principle of thermoelectronic generators without (left) and with (right) a gate. The gate, positively biased with $V_{\rm ge} = 6\,{\rm V}$, is mounted between emitter and collector; a homogeneous magnetic field is applied in x-direction. (a) Calculated profile of the total electrostatic potential. Near the gate, the space-charge potential equals $\sim -2\,{\rm V}$, which in combination with the gate potential of $+6\,{\rm V}$ results in a total potential of $\sim +4\,{\rm V}$. (b) Calculated density of electrons in the space-charge cloud. These electrons do not reach the collector. (c) Calculated density of electrons in the emitter–collector current. These electrons do reach the collector. The calculations and figures refer to the following parameters: $\phi_{\rm e} = 2.5\,{\rm eV}$, $\phi_{\rm c} = 0.9\,{\rm eV}$, $T_{\rm e} = 1227\,^\circ{\rm C}$ (1500 K), $T_{\rm c} \le 250\,^\circ{\rm C}$, $d_{\rm ec} = 100\,{\rm l m}$, $V_{\rm out} = (\phi_{\rm e} - \phi_{\rm c})/e$, $w \to 0$. The labels "$\mathtt{m}_{\rm e}$" and "$\mathtt{m}_{\rm c}$" refer to the electrochemical potentials of the emitter and collector; "$h\nu$" designates the incoming photons; "c", "g", "e", "v" denote the collector, gate, emitter, and vacuum locations, respectively. The data shown here were calculated using the 1D model (see Appendix C 1).

II. RESOLVING THE SPACE-CHARGE PROBLEM WITH ELECTRIC AND MAGNETIC FIELDS

A. Principle of operation and experimental results

Here we show that the space-charge problem can be solved in a plasma-free process. This process involves only electrons but no ions. It is therefore best characterized as "thermoelectronic". To remove the static space charges, a positively charged gate electrode is inserted into the emitter–collector space to create a potential trough. In a virtually lossless process this trough accelerates the electrons away from the emitter surface and decelerates them as they approach the collector (Fig. 1). A nominally homogeneous magnetic field H applied along the electron trajectories prevents loss of the electrons to a gate current I_g by directing them through holes in the gate on helical paths circling straight axes. This process turns the static space-charge cloud, which previously blocked the electron emission, into a useful output current (Figs. 1(b) and 1(c)). The design is analogous to that of ion thrusters used for spacecraft propulsion.

To investigate the effectiveness of the gate in removing the space charges, we fabricated a set of thermoelectronic generators as model systems (Figs. 2(a) and 2(b); see Appendix A). As a first step, we studied the effect of the magnetic field, which we found to indeed prevent electrons from reaching the gate. Without a magnetic field applied, most electrons hit the gate and yield a gate current I_g (Fig. 3(a)). An applied longitudinal magnetic field, however, guides most electrons to the collector. In this case, the ratio of the output current and the total emitted current $I_{ec}/(I_{ec} + I_g)$ almost equals the geometrical transparency t of the gate, the fraction of the

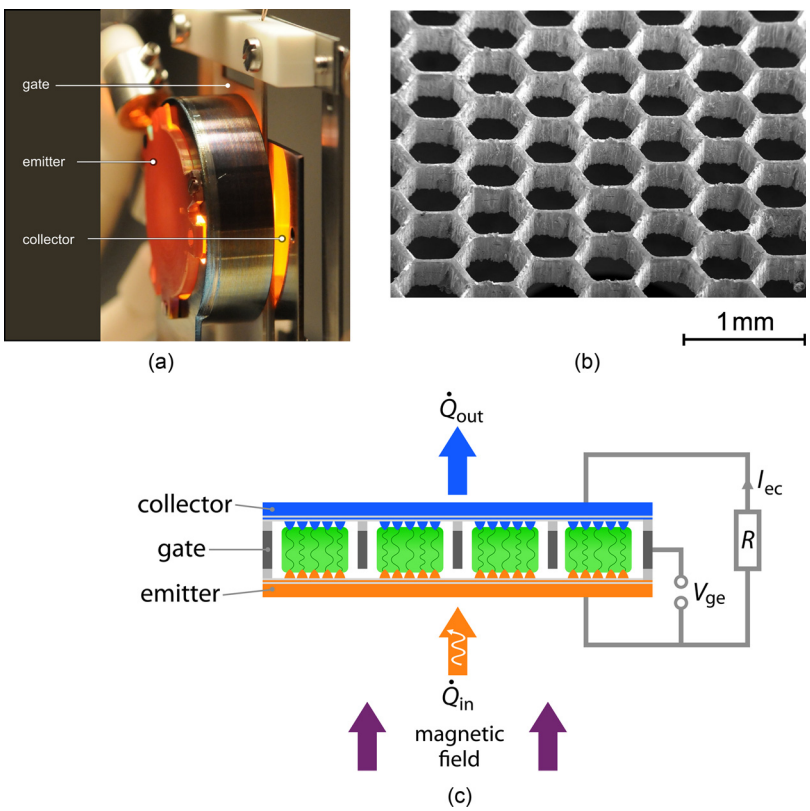

FIG. 2. (a) Photograph of a generator used in these experiments. The glowing orange disk (left) shows the back of the resistively heated emitter (BaO dispenser); the yellowish disk edge on the right shows the reflection of the glowing emitter on the collector surface (steel). (b) Micrograph of a grid (200-㎜-thick tungsten foil, $w = 0.6$ mm) used as gate. (c) Setup of a possible microfabricated generator. The emitter and collector consist of wafers coated with heterostructures (gray lines) designed for the desired work function, thermal and infrared properties. The emitter and collector surfaces comprise nanohillocks for local field enhancements. The green areas mark the regions of the electron flow through the vacuum, the direction of I_{ec} corresponds to the flow of positive charges.

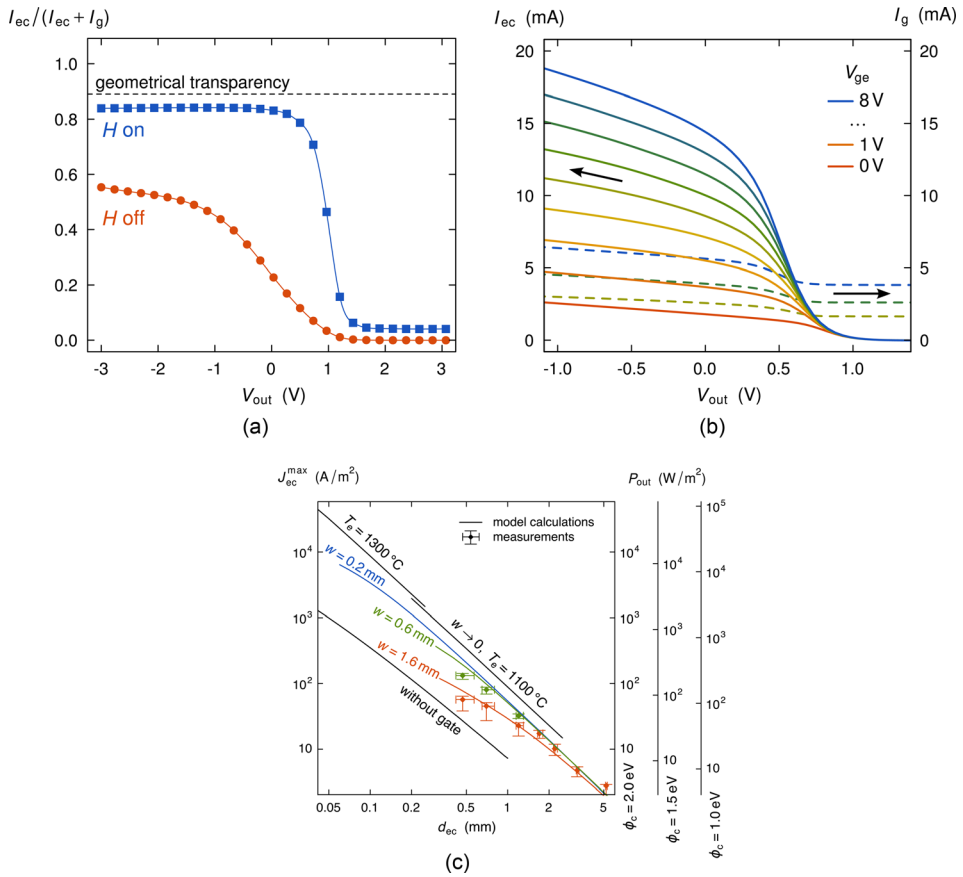

FIG. 3. (a) Ratio of the output current density I_{ec} and the total emitted current density $(I_{ec}+I_g)$ measured as a function of the output voltage V_{out} with (blue) and without (red) a magnetic field (∼200 mT) applied in longitudinal direction ($V_{ge}=6$ V, $T_e=1100$ °C, $w=1.6$ mm, and $d_{ec}=1$ mm for both cases). (b) Output current and gate current measured as a function of V_{out} for several gate voltages at $T_e=1000$ °C, $T_c=500$ °C, $w=1.6$ mm and $d_{ec}=700$ 1m. Nominally identical BaO dispenser cathodes ($\phi_e\sim\phi_c\sim 2.2$ eV) were used for the emitter and collector. (c) Measured and calculated dependences of J_{ec}^{max} on d_{ec}. The data was measured at $T_e=1100$ °C, $T_c\sim 500$ °C, $V_{ge}=6$ V; the calculated current density refers to the density within the gate mesh. The output power densities P_{out} were calculated from J_{ec}^{max} for $\phi_e=3$ eV using $P_{out}=J_{ec}^{max}(\phi_e-\phi_c)/e$. The error bars refer to the errors in determining ϕ_e, ϕ_c, and d_{ec}. The data for $w\to 0$ and for the curve labeled "without gate" were calculated using the 1D model including the thermal distribution of electron velocities (see Appendix C 1); the data for $w>0$ were calculated using the quasi-3D model (see Appendix C 2).

gate area not covered by the conductor. The difference is due to the finite radii of gyration of the electrons and to inhomogeneities of the electric field. For $H\to\infty$ and a homogeneous electric field, $I_{ec}/(I_{ec}+I_g)$ approaches t.

The function of the generators was furthermore modeled by numerical calculations of the electron emission, space-charge formation, and electron trajectories (see Appendix C). Experiment and model calculations provide consistent evidence that, by applying emitter-gate voltages of $V_{ge}\sim 2-10$ V, the exact value being a function of the geometrical design of the generator, the static space-charge clouds are indeed removed (Figs. 1(b), 1(c) and 3(b)). The gate potential enables operation of the generators in vacuum with emitter–collector spacings of tens of micrometers (see Fig. 3(c)).

Although, as will be shown below, the generators operate with high efficiencies at large d_{ec}, the value of the emitter–collector current I_{ec} decreases with d_{ec}. This is illustrated by Fig. 3(c), which shows that the density J_{ec}^{max} of the emitter–collector current at which the maximal output power is obtained, I_{ec}^{max}, scales for large d_{ec} with $1/d_{ec}^2$. At small d_{ec}, J_{ec}^{max} approaches the current density of gate-free generators, because the electric field becomes small

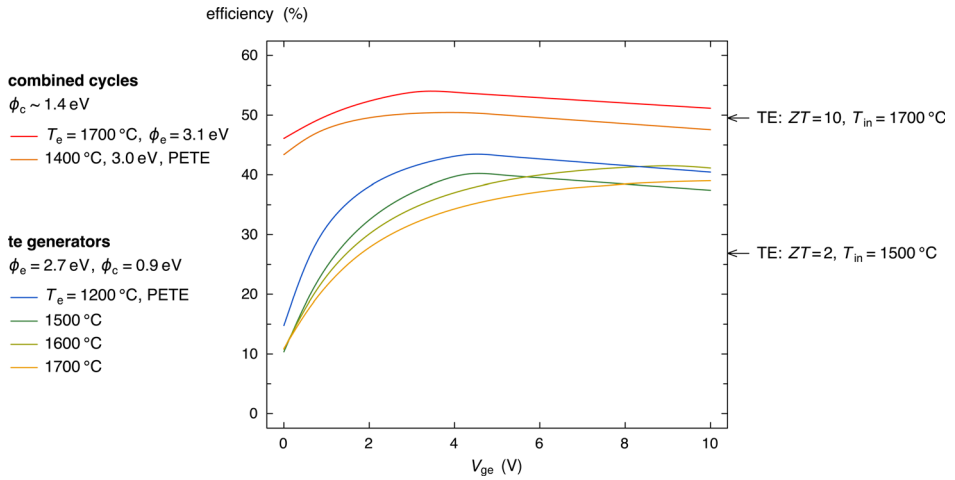

FIG. 4. Heat–to–electric-power conversion efficiencies calculated as a function of the gate voltage V_{ge} of stand-alone thermoelectronic generators working at a series of emitter temperatures ($T_c = 200\,°C$) and of systems comprising a thermoelectronic generator as topping cycle ($d_{ec} = 30\,\mu m$). In the combined-cycle systems, the thermoelectronic generators operate between T_e and $T_s = 600\,°C$. The work functions were selected for optimal performance and $T_e = 1700\,°C$ to allow a comparison with the efficiency given for the stand-alone system. State-of-the-art steam turbines were presumed to work as bottom cycle, receiving heat at T_s and converting it into electricity with $\eta = 45\,\%$. Owing to the high T_{out} of the thermoelectronic generator, ϕ_e and ϕ_c can have rather large values. For the calculation of the efficiencies of the thermoelectronic PETE analogue, a band gap of 1.5 eV and electron affinities of 1.6 eV and 1.85 eV were considered for the stand-alone and the combined-cycle systems, respectively (see Appendix C 3). Light–to–electric-power conversion efficiencies for a light-concentration of 5000 are shown for the PETE systems. The image also lists the efficiencies of hypothetical thermoelectric generators with figures of merit of $ZT = 2$ and 10 at temperatures between T_{in} and 200 8C (see Ref. [25] and Appendix C 3). For comparison, the maximum efficiency of single-junction solar cells is ~34 % (Shockley–Queisser limit[41]) and the best research multi-junction photovoltaic cells have efficiencies of ~43.5 %.[24]

inside the mesh holes if $d_{ec} \ll w$, where w is the grid-mesh diameter defined for hexagonal grids as the distance between opposite corners. For grids with finite conductor widths, I_{ec}^{max} is furthermore reduced because for $t < 1$, a fraction of the emitted current is lost to I_g. This effect can be minimized by optimizing the gate geometry and by inducing an inhomogeneous electron emission, for example by using nanotubes[20] grown on the emitter. In the latter case, I_{ec}^{max} may be increased further by gate-field-enhanced emission.

B. Efficiency limit of thermoelectronic converters

Having confirmed that the space-charge cloud has been removed, we now explore the efficiency $\eta = P_{out}/\dot{Q}_{in}$, with which these generators transform heat into electric power. The output power of the generator, $P_{out} = I_{ec}V_{out}$, is maximal for $V_{out} = (\phi_e - \phi_c)/e$, where ϕ_e and ϕ_c are the work functions of the emitter and the collector,[21] respectively, and e is the elementary charge. For larger V_{out}, some of the electrons lack the energy to reach the collector, whereas I_{ec} is independent of V_{out} for smaller V_{out}. We start to identify the efficiency limit by considering a simplified, ideal case, in which the input power $\dot{Q}_{in}$ is converted completely into an emitter–collector current consisting only of electrons at the vacuum potential ($E = 0$). If the electrons are only thermally emitted, the requirement that the back-emission current from the collector is so small that I_{ec}^{max} is positive entails that $\eta < 1 - T_c/T_e$ (see Appendix C 3). To generate this ideal current, a power of $\dot{Q}_{in} = I_{ec}^{max}\phi_e/e$ is required. Therefore, $\eta_{max} = 1 - \phi_c/\phi_e$ is a strict upper limit for the heat–to–electric power conversion efficiency. This limit also applies to devices in which the photoelectric effect is used.

C. Projected efficiencies

In real devices, η is reduced by several loss channels, which include the above-neglected thermal energy carried from the emitter by I_{ec}^{max}, losses due to a finite I_g, radiation losses from

the emitter, thermal conduction of the wires contacting the electrodes, and ohmic losses. Nevertheless, only the loss by the electron heat current causes a fundamental bound for the efficiency; the other loss effects can in principle be reduced to very small values.

Figure 4 shows the results of the model calculations of the generator efficiencies as a function of the gate voltage, considering the above-mentioned losses (see Appendix C 3). Starting at $V_{ge} = 0$, η increases with V_{ge} as the gate potential sweeps the space charges into the collector. This increase demonstrates the usefulness of the gate field. At higher $V_{ge,}$ η decreases because the space charges have been removed and V_{ge} does not enhance I_{ec}^{max} beyond the maximum emission current, but increases the power $I_g V_{ge}$ lost at the gate. For a given V_{ge} the effect of the space charge can only be efficiently suppressed for I_{ec}^{max} not exceeding an upper limit. By enhancing T_e this upper limit can only be increased slightly. Consequently, for a given V_{ge} it is preferable to choose T_e such that the maximum emission current equals the upper limit defined by $V_{ge.}$ Higher T_e result in higher thermal losses rather than enhancing I_{ec}^{max}, while lower T_e reduce I_{ec}^{max}.

For the parameter range considered realistic for applications (*e.g.*, $d_{ec} = 30\,\mu m$, $t = 0.98$, $\phi_c = 0.9\,eV$),[22] maximum efficiencies of $\sim 42\,\%$ are predicted. The calculated maximum efficiencies (Fig. 4) are consistent with previous calculations of efficiencies of thermionic generators that were presumed to be devoid of space charges.[2,10,15,16,23] They compare well with those of photovoltaic solar cells,[24] thermoelectric materials,[25,26] and focused solar mechanical generators.[27,28] The results on combined cycles shown in Fig. 4 reveal that by using thermoelectronic converters as topping cycles the efficiency of state-of-the-art coal combustion plants may be increased from 45 % to 54 %, corresponding to a reduction of emissions such as CO_2 by $\sim 17\,\%$.

III. CONCLUSION

Based on our experimental and theoretical work we conclude that the combination of gate electrodes and longitudinal magnetic fields allows the fabrication of thermoelectronic generators that efficiently convert heat into electric power. Optimization of the conversion efficiencies requires the development of metal or semiconductor surfaces with the desired effective work functions and electron affinities, respectively, which may also be done by nanostructuring the electrode surfaces. These surfaces need to be stable at high temperatures in vacuum. The tunability of the gate field opens possibilities to alter the converter parameters during operation. Although the need to generate Cs^+ ions to neutralize the space-charge cloud is eliminated, adatoms of elements such as Cs can be used to lower the work function of the electrodes, in particular of the collector. For high efficiency, the devices must be thermally optimized to minimize heat losses through the wiring. Furthermore, thermal radiation of the emitter must be reflected efficiently onto the electrode. For ballistic electron transport between emitter and collector, a vacuum of better than 0.1 mbar is also required, reminiscent of radio tubes (compare Appendix B).

Such devices may be realized, for example, in a flip-chip arrangement of micromachined emitter and collector wafers separated by $\sim 10 - 100\,\mu m$ using a microfabricated gate with holes of comparable or slightly smaller sizes, and ceramic spacers, such as Al_2O_3 films, for thermal insulation as sketched in Fig. 2(c). The emitter and collector surfaces are preferably coated to optimize their work functions and infrared emission and absorption properties. The surfaces may furthermore be equipped with nanostructures, *e.g.*, with nanotubes,[20] to optimize the emission and absorption properties for electrons and photons. To achieve sufficient electron mean free paths, background pressures < 0.1 mbar are required (see Appendix B). According to the calculations presented, such devices may produce hundreds of Watts of power from active areas of some $100\,cm^2$. The magnetic fields, typically $\leq 1\,T$ with large tolerances in strength and spatial distribution, can be generated by permanent magnets or, for applications such as power plants, by superconducting coils. Achieving viable, highly-efficient devices requires substantial further materials science efforts to develop the functional, possibly nanostructured materials, as well as engineering efforts to achieve a stable vacuum environment in order to minimize radiative and conductive heat losses, and to ensure competitive costs. Remarkably, however, no obstacles of a fundamental nature appear to impede highly efficient power generation based on thermoelectronic energy converters.

TABLE I. Approximate mean free path of electrons for a series of base pressures calculated as in Ref. 31. These values are a good approximation for most residual gases at $T_{gas} = 1000\,K$.

pressure	mean free path	maximal gap width
1000 mbar	2 mm	20 nm
10 mbar	200 mm	2 mm
0.1 mbar	2 cm	200 mm
10^{-3} mbar	2 m	2 cm

ACKNOWLEDGMENTS

The authors gratefully acknowledge discussions with H. Boschker, R. Kneer, T. Kopp, H. Queisser, A. Reller, H. Ruder, A. Schmehl, and J. Weis as well as technical support by B. Fenk and A. Herrnberger. One of us (T.H.G.) would like to acknowledge informative conversations on the use of triodes with longitudinal magnetic fields to generate Cs plasmas in thermionic generation with the late Boris Moyzhes, and also would like to acknowledge support for part of the work at Stanford by the U.S. Department of Energy, under contract DE-DE-AC02-76SF00515.

APPENDIX A: EXPERIMENTAL SETUP AND PROCEDURES

In the model systems the electrodes were mechanically mounted in a vacuum chamber (base pressure 10^{-7} mbar) to facilitate the study of various converter configurations. As emitters, commercial, resistively heated BaO-dispenser cathodes[29] with a temperature-dependent work function in the range $2.0\,eV < \phi_e < 2.5\,eV$ and an emitting area of $2.8\,cm^2$ were used. The gates were laser-cut tungsten foils, the spacers aluminum oxide foils, and the collectors either consisted of polished steel plates or were BaO-dispenser cathodes. The collector work functions were determined from the $I_{ec}(V_{out})$-characteristics and additionally from the Richardson-Dushman saturation current[30] (also see Appendix C 3). The emitters are ohmically heated, T_e was measured with a pyrometer. The magnetic field is generated by two stacks of NdFeB permanent magnets mounted on both sides of the emitter-gate-collector assembly. They created at the gates $\sim(200 \pm 10)\,mT$. Photon-enhancement of the emission was not applied. Electrical measurements were performed with source-measurement units (Keithley 2400) in 4-wire sensing.

APPENDIX B: ELECTRON MEAN FREE PATH AND REQUIRED BASE PRESSURE

The mean free path λ of electrons in presence of residual gas molecules of temperature T_{gas} and pressure p scales as $\lambda \propto T_{gas}/p$.[31]

Assuming that no more than 1% of the emitted electrons should be involved in collisions, the maximum allowed gap width can be estimated from the mean free path. As Table I illustrates, a base pressure of 0.1 mbar is sufficient for efficient thermoelectronic energy conversion.

Apart from that, low base pressures will usually be preferable to stabilize the surfaces of the emitter and collector electrodes and to prevent parasitic heat transport.

APPENDIX C: MODEL CALCULATIONS

1. One-dimensional models

For the calculations of the current densities in gate-free, plane-parallel configurations the one-dimensional space-charge theory of Langmuir[32] and Hatsopoulos[33] was used to determine the space-charge potential. To incorporate the effect of the gate in the one-dimensional approach, these models were extended to include the potential generated by an idealized gate, assumed to be

a metal plate that is transparent for electrons and to create a homogeneous electric field. Calculations of the electric field of a patterned metal grid with the commercial electric field solver COULOMB[34] showed that for $d_{ec} > w$ the generated field is virtually identical to the field of an idealized gate. The 3D calculations of the electric field distribution and the electron paths in the electric gate field and the applied magnetic field done with the commercial software LORENTZ[34] showed that the electrons are forced on quasi-one dimensional paths by the magnetic field and are thus channeled through the gate openings.

To explore J_{ec}^{max} as a function of V_{ge} below we calculate the course of the electric potential in the vacuum gap. For this we consider a symmetrical setup, the gate being located in the middle between emitter and collector. The gate potential for electrons is given by

$$\varphi_g(x) = -\frac{2V_{ge}}{d_{ec}}x \quad \text{for } 0 \le x \le \frac{d_{ec}}{2},$$

and

$$\varphi_g(x) = -\frac{2V_{ge}}{d_{ec}}(d_{ec} - x) \quad \text{for } \frac{d_{ec}}{2} \le x \le d_{ec}.$$

At maximum power output, emitter and collector have the same local vacuum potential. We assume the collector to be cold enough that back emission is negligible, as discussed in Ref. 33.

If the thermally distributed initial velocity of emitted electrons is neglected, the Poisson equation is given by

$$\mathrm{DW}(x) = -\frac{J_{ec}^{max}}{\epsilon_0}\left(-\frac{2e}{m_e}\mathrm{W}(x)\right)^{-1/2},$$

where $\mathrm{W}(x)$ is the total electrostatic potential for negative charges, consisting of the contribution of the gate and the space-charge potential. This equation is solved analytically, analogous to the Child-Langmuir law,[35,36] yielding

$$J_{ec}^{max} = \epsilon_0\sqrt{\frac{e}{6m_e}}\frac{{V_{ge}}^{3/2}}{d_{ec}^2}. \tag{C1}$$

Remarkably, the current density shows the same behavior $J_{ec}^{max} \propto {V_{ge}}^{3/2}/d_{ec}^2$ as the Child-Langmuir law.

If the thermal velocity distribution is included, the Poisson equation becomes

$$\mathrm{DW}(x) = -\frac{en_0}{\epsilon_0}\exp\left[-\frac{e}{k_B T_e}\mathrm{W}(x)\right]\cdot\left\{1 \pm \mathrm{erf}\left[\frac{e}{k_B T_e}\left(\mathrm{W}_{max} - \mathrm{W}(x)\right)\right]\right\},$$

where en_0 is the space-charge density at the emitter surface and W_{max} the maximum of the space-charge potential in the inter-electrode space. The plus sign is valid for $x \le x_{max}$, the minus sign for $x \ge x_{max}$, with x_{max} being the position of W_{max}. n_0 can be determined from the Richardson-Dushman equation,[33] it is a function of ϕ_e and T_e. This self-consistent differential equation has to be solved numerically.

We used Mathematica 8.0 for the numerical calculations. For each iteration step, the change of the space-charge potential has to be kept small, as already a small modification of $\mathrm{W}(x)$ can lead to a strong modification or even a divergence of the solution. Therefore, the solution has to be approached slowly to impede a strong oscillatory behavior.

The model calculations labeled "$w \to 0$" in Fig. 3(b) were obtained using the ideal transparent gate model including the electron velocity distribution.

2. The quasi-3-dimensional current tube model

To take the inhomogeneities of the electric field of the gate electrode into account, the interelectrode space was subdivided into narrow prisms, which extend from the emitter to the collector

surface. We calculated the average gate potential in each prism with the electric field solver COULOMB.[34] We apply a linear regression to determine the mean electric field, which can be used in the one-dimensional gate model. We then calculate the current density for each prism separately. Thereby the interactions between the prisms were neglected, which is a good approximation for the case of small inhomogeneities in the space-charge density. The total current density was obtained by summing up the contributions from all tubes.

Due to the high computational effort required to solve the 1D model including the thermally distributed initial electron velocity, the analytical solution (Eq. (C1)) was used to determine the current density, which yields a good approximation in the voltage range considered. However, it does not account for the temperature-dependence of the current density.

3. Efficiency calculations

a. Calculation of the ultimate efficiency limit

The Richardson-Dushman equation describes the current density for electrons emitted from a metal surface.[30] It is obtained by using the equation $J = -nev$ and integrating the Fermi distribution f_{FD} over all electrons with a positive velocity normal to the emitting surface, *i.e.*,

$$J_{\mathrm{RD}} = -e\int_{\mathsf{v}_x>0}\int\int \mathrm{d}\vec{\mathsf{v}}\,\mathsf{v}_x f_{\mathrm{FD}}(\vec{\mathsf{v}}) \approx \frac{em_{\mathrm{e}}}{4\pi^2\hbar^3}\exp\left(\frac{-\phi}{k_{\mathrm{B}}T}\right)\cdot\int_0^\infty \mathrm{d}\mathsf{v}_x\int_{-\infty}^{\infty}\mathrm{d}\mathsf{v}_y\int_{-\infty}^{\infty}\mathrm{d}\mathsf{v}_z\mathsf{v}_x\exp\left(\frac{-m_{\mathrm{e}}\mathsf{v}^2}{2k_{\mathrm{B}}T}\right)$$
$$= -A_{\mathrm{RD}}T^2\exp\left(\frac{-\phi}{k_{\mathrm{B}}T}\right). \tag{C2}$$

A_{RD}: Richardson-Dushman constant, ϕ: work function, T: surface temperature, v: electron velocity.

If all non-fundamental channels of heat loss are neglected, heat is lost from the emitter only by the transport of electrons. This electron cooling $\dot{Q}_{\mathrm{el}}$ is given by[33]

$$\dot{Q}_{\mathrm{el}} = \int_0^\infty \mathrm{d}\mathsf{v}_x\int_{-\infty}^{\infty}\mathrm{d}\mathsf{v}_y\int_{-\infty}^{\infty}\mathrm{d}\mathsf{v}_z\mathsf{v}_x\left(\phi_{\mathrm{e}}+\frac{m_{\mathrm{e}}\mathsf{v}^2}{2}\right)f_{\mathrm{FD}}(\mathsf{v}) = \frac{J_{\mathrm{RD}}}{e}(2k_{\mathrm{B}}T_{\mathrm{e}}+\phi_{\mathrm{e}}). \tag{C3}$$

Assuming there is no space-charge cloud limiting the transfer of electrons across the vacuum gap, both the current density $J_{\mathrm{e}}^{\max}$ emitted from the emitter and the back-emission $J_{\mathrm{be}}^{\max}$ emitted from the collector are given by the respective Richardson-Dushman current densities (Eq. (C2)).

Taking into account the heat transported back to the emitter by the back-emission, the efficiency is obtained to be

$$\eta = \frac{J_{\mathrm{ec}}^{\max}(\phi_{\mathrm{e}}-\phi_{\mathrm{c}})}{J_{\mathrm{e}}^{\max}(\phi_{\mathrm{e}}+2k_{\mathrm{B}}T_{\mathrm{e}})-J_{\mathrm{be}}^{\max}(\phi_{\mathrm{e}}+2k_{\mathrm{B}}T_{\mathrm{c}})}. \tag{C4}$$

This value is known to always be smaller than the Carnot efficiency.[3,19]

However, the efficiency may be ultimately increased if electrons are emitted only at a discrete energy E_0, so that the $2k_{\mathrm{B}}T$-terms in Eqs. (C3) and (C4) disappear. For this case, however, the Richardson-Dushman equation does not apply. Instead, the emitted current density has to be calculated for a hypothetical material with the discrete energy level E_0, from which the emission of electrons occurs. This level may be at or above the vacuum level. This calculation can be performed by inserting a δ-function to describe the discrete density-of-states at $E = E_0$. In this case, in Eq. (C2) no Gaussian-integral has to be determined and the resulting, discrete current density does not have a term with coefficient T^2.

As for any thermoelectronic generator, an output power is only generated for

$$J_{ec}^{max} = J_{e}^{max} - J_{be}^{max} = J_{e,E0}^{max} - J_{be,E0}^{max} > 0,$$

implying

$$\exp\left(\frac{-\phi_e}{k_B T_e}\right) - \exp\left(\frac{-\phi_c}{k_B T_c}\right) > 0.$$

It follows

$$\frac{\phi_c}{\phi_e} > \frac{T_c}{T_e}$$

and therefore

$$\eta = \frac{J_{ec}^{max}/e \cdot (\phi_e - \phi_c)}{J_{ec}^{max}/e \cdot \phi_e} = \frac{\phi_e - \phi_c}{\phi_e} = 1 - \frac{\phi_c}{\phi_e} < 1 - \frac{T_c}{T_e} = \eta_{Carnot}.$$

For $J_{ec}^{max} \to 0$, it follows:

$$\frac{\phi_c}{\phi_e} \to \frac{T_c}{T_e}$$

and consequently

$$\eta \to \eta_{Carnot}.$$

As can be seen, the efficiency approaches the Carnot limit if the net current across the vacuum gap approaches zero, *i.e.*, if the system approaches equilibrium. Consequently, the output power approaches zero when the efficiency approaches the Carnot limit. This is a very typical behavior for any realistic heat engine (see, *e.g.*, Refs. 37 and 38).

b. Stand-alone generators

To calculate the efficiency of realistic thermoelectronic generators, the calculations presented in Refs. 2, 16, and 23 were extended to include both the gate energy loss and the dependence of I_e^{max} on the gate voltage. In determining the generator efficiency, the power P_g required to sustain the gate electric field is subtracted from the output power

$$\eta = \frac{P_{out} - P_g}{\dot{Q}_{in}},$$

where $\dot{Q}_{in}$ is the heat input and P_{out} the power delivered to the load. It is given by

$$P_{out} = \left(\frac{\phi_e - \phi_c}{e} - V_{lead}\right) I_{ec}^{max},$$

with the net current flowing to the collector

$$I_{ec}^{max} = tI_{e}^{max} - I_{be}^{max}$$

and the voltage drop in the leads connecting the load with the emitter (R_{le}) and collector (R_{lc})

$$V_{lead} = I_{ec}^{max} R_{lc} + (I_{e}^{max} - tI_{be}^{max}) R_{le}.$$

Here, I_e^{max} is the space-charge limited current emitted from the emitter, which is calculated from the models described above and I_{be}^{max} the back-emission current emerging from the collector. It has

to be considered that I_{be}^{max} is also reduced by the space-charge potential. Therefore, it is given by

$$I_{be}^{max} = I_{RD} \exp\left(-\frac{W_{max}}{k_B T_c}\right),$$

with the Richardson-Dushman current I_{RD} (Eq. (C2)) and the maximum of the inter-electrode potential W_{max}.

In the steady state the heat input equals the sum of all channels of heat loss from the emitter

$$\dot{Q}_{in} = \dot{Q}_{el} + \dot{Q}_{rad} + \dot{Q}_{cond},$$

with the electron cooling

$$\dot{Q}_{el} = \frac{I_e^{max}}{e}(\phi_e + W_{max} + 2k_B T_e) - \frac{tI_{be}^{max}}{e}(\phi_e + W_{max} + 2k_B T_c), \tag{C5}$$

the radiation cooling

$$\dot{Q}_{rad} = \sigma \epsilon A({T_e}^4 - t{T_c}^4),$$

(A: emitter area, σ: Stefan-Boltzmann constant, $\epsilon \sim 0.1$: effective emissivity of the electrode system)[16] and the heat conduction across the emitter lead

$$\dot{Q}_{cond} = \frac{L}{2R_{le}}(T_e - T_0)^2 - \frac{R_{le}}{2}(I_e^{max} - tI_{be}^{max})^2,$$

where the lead is assumed to be metallic and to follow the Wiedemann-Franz law. With the Lorentz number L the thermal conductivity can consequently be expressed as $L(T_e - T_0)/(2R_{le})$. The load is assumed to be at ambient temperature T_0. The second term in this equation arises from half of the Joule heat produced in the lead effectively being transported to the emitter, which can be shown by solving the heat flow equation.[2]

c. Combined-cycle systems

In combined cycle systems the heat rejected by the collector ($\dot{Q}_{out}$) is used to drive a secondary heat engine working at an efficiency η_s. The power $\eta_s \dot{Q}_{out}$ produced by this engine is added to the total produced power, hence

$$\eta_{cc} = \frac{P_{out} - P_g + \eta_s \dot{Q}_{out}}{\dot{Q}_{in}}.$$

In the steady state $\dot{Q}_{out}$ is equivalent to the heat transported to the collector, given by the sum of an electronic, radiation, and conduction term

$$\dot{Q}_{out} = \dot{Q}_{elc} + \dot{Q}_{radc} + \dot{Q}_{condc},$$

where

$$\dot{Q}_{elc} = \frac{tI_e^{max}}{e}(\phi_c + W_{max} + 2k_B T_e) - \frac{I_{be}^{max}}{e}(\phi_c + W_{max} + 2k_B T_c),$$
$$\dot{Q}_{radc} = \sigma \epsilon A(t{T_e}^4 - {T_c}^4), \tag{C6}$$

and

$$\dot{Q}_{\mathrm{condc}} = -\frac{L}{2R_{\mathrm{lc}}}(T_{\mathrm{c}} - T_0)^2 + \frac{(I_{\mathrm{ec}}^{\max})^2 R_{\mathrm{lc}}}{2}.$$

d. Losses specific to solar heating

For solar heated thermoelectronic generators another fundamental channel for heat loss arises which we take into account: to couple solar radiation into the emitter, the emitter needs to provide a highly absorbing surface A_{b} (here "b" stands for black). This surface A_{b} has a high emissivity and therefore emits a thermal power. The resulting, reduced light–to–electricity efficiency η_{l} is expressed in terms of the heat–to–electricity efficiency η

$$\eta_{\mathrm{l}} = \left(1 - \frac{\sigma {T_{\mathrm{e}}}^4}{cI_0}\right)\eta,$$

where c is the concentration-factor of the incoming solar radiation onto the absorbing spot on the emitter[39] and I_0 the intensity of the incoming solar radiation.

e. PETE-efficiencies

To calculate the efficiency of a PETE device incorporating a gate electrode, we first assume a given emitted current density $J_{\mathrm{e}}^{\mathrm{PETE}}$ and emitter temperature T_{e}. The latter is chosen such that the hypothetical Richardson-Dushman current density across the electron-affinity barrier (E_{a}) is at least 100 times larger than $J_{\mathrm{e}}^{\mathrm{PETE}}$. For an ideal PETE-device we then expect an electron yield of 1 electron per above-bandgap-photon,[4] as photoexcited electrons can then be assumed to be thermally emitted significantly faster than they recombine.

From $J_{\mathrm{e}}^{\mathrm{PETE}}$, which defines the emission capability of the emitter, we then calculate the space-charge limited current density $J_{\mathrm{ec}}^{\max}$ from the 1D model described above (taking into account the thermally distributed starting velocity of the electrons). This defines the input power actually required to maintain a stable emitter temperature and, consequently, the required incident light concentration c_{eff}. For the data shown, this typically yields $c_{\mathrm{eff}} \sim 500$. To satisfy the self-consistency, from c_{eff} and $J_{\mathrm{ec}}^{\max}$ we finally calculate the bandgap D that yields the required rate of photoexcitations into the conduction band.

We assume the chemical potential to be in the middle between the worst case (middle of the bandgap) and the best case (bottom of the bandgap). Consequently, the emitter work-function is

$$\phi_{\mathrm{e}} = E_{\mathrm{a}} + \frac{3}{4}\mathrm{D}.$$

From ϕ_{e} and $J_{\mathrm{ec}}^{\max}$ the efficiencies of both stand-alone and combined-cycle PETE devices can be calculated as described above.

f. Intrinsic electronic heat losses

Below, the relative importance of the channels of heat loss will be discussed for the peak of the efficiency of the 16008C curve shown in Fig. 4. Although the resulting numbers may slightly vary for other configurations, the ratios of the different contributions remain essentially the same.

At the peak of the efficiency of the 16008C curve shown in Fig. 4 the total input power of $\dot{Q}_{\mathrm{in}} = 78.1\,\mathrm{W/cm^2}$ is mainly consumed by the electron cooling of $\dot{Q}_{\mathrm{el}} = 67.3\,\mathrm{W/cm^2}$. Therefrom, $60.0\,\mathrm{W/cm^2}$ are consumed by the emitted electrons to overcome ϕ_{e} and $7.3\,\mathrm{W/cm^2}$ arise from the thermally distributed electron velocity (the $2k_{\mathrm{B}}T$-terms in Eqs. (C5) and (C6)). The remaining loss splits up between thermal radiation ($\dot{Q}_{\mathrm{rad}} = 7.0\,\mathrm{W/cm^2}$) and conduction across the lead wires ($\dot{Q}_{\mathrm{cond}} = 3.8\,\mathrm{W/cm^2}$). In this configuration the system delivers a power of $P_{\mathrm{out}} = 36.4\,\mathrm{W/cm^2}$ to the load cycle, while $P_{\mathrm{g}} = 4.0\,\mathrm{W/cm^2}$ are consumed on the gate. The resulting net output power of $32.4\,\mathrm{W/cm^2}$ corresponds to an efficiency of $\eta = 42\,\%$.

g. Efficiency of thermoelectric generators

For comparison, efficiencies of hypothetical thermoelectric generators are given in Fig. 4. Those were calculated following, *e.g.*, Ref. 26,

$$\eta = \left(1 - \frac{T_{\text{out}}}{T_{\text{in}}}\right) \frac{\sqrt{1+ZT} - 1}{\sqrt{1+ZT} + T_{\text{out}}/T_{\text{in}}}.$$

Using this formula we calculated the efficiency of thermoelectric devices with specific ZT-values and inlet temperatures. To compare thermoelectric and thermoelectronic generators $T_{\text{out}} = T_{\text{c}} = 200\,^{\circ}\text{C}$ was selected.

APPENDIX D: NOMENCLATURE OF VARIABLES

A	emitter area
A_{b}	absorbing surface used for solar heating of generator
A_{RD}	Richardson-Dushman constant
c	concentration factor of solar radiation focused onto the light-absorbing area of the emitter
c_{eff}	effective concentration factor of solar radiation[39]
d_{ec}	emitter-collector distance
e	absolute value of the elementary charge
E	total energy of electrons
E_0	a hypothetical, discrete energy level from which electrons are emitted used to obtain the ultimate efficiency limit
E_{a}	semiconductor electron affinity
f_{FD}	Fermi-Dirac distribution function
H	magnetic field strength
$\hbar$	reduced Planck constant
I_0	intensity of the incoming, not yet focused, solar radiation
$I_{\text{be}}^{\text{max}}$	back-emitted current at maximal power
I_{ec}	emitter-collector current
$I_{\text{ec}}^{\text{max}}$	emitter-collector current at maximal power
$I_{\text{e}}^{\text{max}}$	current emitted from the emitter at maximal power
I_{g}	gate current
$J_{\text{be}}^{\text{max}}$	back-emitted current density at maximal power
$J_{\text{be,E0}}^{\text{max}}$	back-emitted current density at maximal power for emission from E_0
$J_{\text{ec}}^{\text{max}}$	emitter-collector current density at maximal power
$J_{\text{e}}^{\text{PETE}}$	photon-enhanced current density emitted from the emitter at maximal power
$J_{\text{e}}^{\text{max}}$	current density emitted from the emitter at maximal power
$J_{\text{e,E0}}^{\text{max}}$	current density emitted from the emitter at maximal power for emission from E_0
J_{RD}	Richardson-Dushman current density
k_{B}	Boltzmann constant
L	Lorentz number
m_{e}	electron mass
n_0	electron number density at the emitter surface
p	pressure
P_{g}	power consumed to maintain the positive charge on the gate
P_{out}	output power
$\dot{Q}_{\text{cond}}$	heat loss from the emitter due to heat conduction across the lead wire
$\dot{Q}_{\text{condc}}$	heat input to the collector due to heat conduction across the lead wire
$\dot{Q}_{\text{el}}$	heat loss from the emitter due to electron emission
$\dot{Q}_{\text{elc}}$	heat input into the collector by electron emission

$\dot{Q}_{\mathrm{in}}$	thermal input power
$\dot{Q}_{\mathrm{out}}$	heat rejected by the collector
$\dot{Q}_{\mathrm{rad}}$	heat loss from the emitter due to thermal radiation
$\dot{Q}_{\mathrm{radc}}$	heat input into the collector by thermal radiation
R_{l}	electrical resistance of the load
R_{lc}	electrical resistance of the wire connecting load and collector
R_{le}	electrical resistance of the wire connecting load and emitter
t	geometrical transparency of the grid mesh
T_0	ambient temperature
T_{c}	collector temperature
T_{e}	emitter temperature
T_{gas}	temperature of the residual gas molecules
T_{in}	inlet temperature of heat engine
T_{out}	outlet temperature of heat engine
T_{s}	inlet temperature of secondary heat engine
V_{ge}	applied gate voltage (with respect to the emitter)
V_{lead}	voltage drop due to non-zero values of R_{le} and R_{lc}
V_{out}	output voltage
w	diameter of the grid meshes, for a hexagonal structure defined by the distance between opposite corners
x	position within the interelectrode space
x_{max}	position of the maximum of W in the interelectrode space
ZT	figure-of-merit of a thermoelectric converter
D	semiconductor bandgap
ϵ	effective emissivity of the electrode system
ε_0	electric constant
η	efficiency of energy conversion
η_{C}	Carnot efficiency
η_{cc}	efficiency of a combined-cycle system
η_{l}	reduced efficiency due to solar heating
η_{max}	upper limit of the efficiency
η_{s}	efficiency of a secondary heat engine
λ	electron mean free path
μ_{c}	electrochemical potential of the collector
μ_{e}	electrochemical potential of the emitter
σ	Stefan-Boltzmann constant
ϕ_{c}	collector work function
ϕ_{e}	emitter work function
φ_{g}	electrostatic potential induced by the gate
W	total electrostatic potential for negative charges
$\mathrm{W}_{\mathrm{max}}$	maximal value of W in the interelectrode space

[1]W. Schlichter, "Die spontane Elektronenemission glühender Metalle und das glühelektrische Element," Ann. Phys. **352**, 573–640 (1915).
[2]J. H. Ingold, "Calculation of the maximum efficiency of the thermionic converter," J. Appl. Phys. **32**, 769–772 (1961).
[3]G. N. Hatsopoulos and E. P. Gyftopoulos, *Thermionic Energy Conversion Volume I: Processes and Devices* (MIT Press, Cambridge and London, 1973).
[4]J. W. Schwede, I. Bargatin, D. C. Riley, B. E. Hardin, S. J. Rosenthal, Y. Sun, F. Schmitt, P. Pianetta, R. T. Howe, Z. Shen, and N. A. Melosh, "Photon-enhanced thermionic emission for solar concentrator systems," Nature Mater. **9**, 762–767 (2010).
[5]G. O. Fitzpatrick, E. J. Britt, and B. Moyzhes, in *Proceedings of the 32nd Intersociety Energy Conversion Engineering Conference IECEC-97 on Updated Perspective on the Potential for Thermionic Conversion to Meet 21st Century Energy Needs* (American Institute of Chemical Engineers, 1997) Vol. 2, pp. 1045–1051.
[6]A. F. Ioffe, *Semiconductor Thermoelements and Thermoelectric Cooling* (Infosearch Ltd. London, London, 1957).
[7]See also Appendix D for a list of all relevant parameters used.
[8]"Key world energy statistics 2012," Technical Report International Energy Agency, 2012.

[9]R. E. Engdahl, A. J. Cassano, and R. B. Dowdell, "Thermionics in fossil-fuel and nuclear central power stations," Combustion **41**, 24 (1970).
[10]B. Y. Moyzhes and T. H. Geballe, "The thermionic energy converter as a topping cycle for more efficient heat engines—new triode designs with a longitudinal magnetic field," J. Phys. D **38**, 782–786 (2005).
[11]G. P. Smestad, "Conversion of heat and light simultaneously using a vacuum photodiode and the thermionic and photoelectric effects," Sol. Energy Mater. Sol. Cells **82**, 227–240 (2004).
[12]G. N. Hatsopoulos and J. Kaye, "Measured thermal efficiencies of a diode configuration of a thermo electron engine," J. Appl. Phys. **29**, 1124–1125 (1958).
[13]H. Moss, "Thermionic diodes as energy converters," J. Electron. Control **2**, 305–322 (1957).
[14]National Research Council, Committee on Thermionic Research and Technology, *Thermionics Quo Vadis? An Assessment of the DTRA's Advanced Thermionics Research and Development Program* (National Academy Press, Washington D.C., 2001).
[15]J. Lee, I. Bargatin, N. A. Melosh, and R. T. Howe, "Optimal emitter-collector gap for thermionic energy converters," Appl. Phys. Lett. **100**, 173904 (2012).
[16]N. S. Rasor, "Thermionic energy-conversion plasmas," IEEE Trans. Plasma Sci. **19**, 1191–1208 (1991).
[17]N. S. Rasor, "Emission physics of the thermionic energy converter," Proc. IEEE **51**, 733–747 (1963).
[18]N. N. Ponomarev-Stepnoi, V. M. Talyzin, and V. A. Usov, "Russian space nuclear power and nuclear thermal propulsion systems," Nucl. News **43**, 33–46 (2000).
[19]F. G. Baksht, G. A. Dyuzhev, A. M. Martsinovskiy, B. Y. Moyzhes, G. Y. Pikus, E. B. Sonin, and V. G. Yur'yev, "Thermionic converters and low-temperature plasma," Technical Report N, Vol. 80 (Technical Information Center/DOE, 1978), pp. 17579.
[20]P. Yaghoobi, M. V. Moghaddam, and A. Nojeh, "Heat trap: Light-induced localized heating and thermionic electron emission from carbon nanotube arrays," Solid State Commun. **151**, 1105–1108 (2011).
[21]Following common usage (*e.g.*, Ref. 40), we define the work function of a material as the energy required to move an electron with an energy equaling the chemical potential from inside the material to a location far away from the surface.
[22]F. A. M. Koeck, R. J. Nemanich, A. Lazea, and K. Haenen, "Thermionic electron emission from low work-function phosphorus doped diamond films," Diamond Relat. Mater. **18**, 789–791 (2009).
[23]J. M. Houston, "Theoretical efficiency of the thermionic energy converter," J. Appl. Phys. **30**, 481–487 (1959).
[24]M. A. Green, K. Emery, Y. Hishikawa, W. Warta, and E. D. Dunlop, "Solar cell efficiency tables (version 40)," Prog. Photovoltaics **20**, 606–614 (2012).
[25]L. E. Bell, "Cooling, heating, generating power, and recovering waste heat with thermoelectric systems," Science **321**, 1457–1461 (2008).
[26]G. J. Snyder and E. S. Toberer, "Complex thermoelectric materials," Nature Mater. **7**, 105–114 (2008).
[27]H. Müller-Steinhagen and F. Trieb, "Concentrating solar power," Ingenia **2004**, 43–50.
[28]*SolarPACES Annual Report 2009*, edited by C. Richter (International Energy Agency, 2010), available from www.solarpaces-csp.org/Library/AnnualReports.
[29]HeatWave Labs, Inc., 195 Aviation Way, Suite 100, Watsonville, CA 95076-2069, USA.
[30]N. W. Ashcroft and N. D. Mermin, *Solid State Physics* (Holt, Rinehart and Winston, New York, 1976).
[31]A. Roth, *Vacuum Technology*, 3rd ed. (Elsevier Science Publishers, Amsterdam, 1990).
[32]I. Langmuir, "The effect of space charge and initial velocities on the potential distribution and thermionic current between parallel plane electrodes," Phys. Rev. **21**, 419–435 (1923).
[33]G. N. Hatsopoulos and E. P. Gyftopoulos, *Thermionic Energy Conversion Volume II: Theory, Technology and Application* (MIT Press, Cambridge and London, 1979).
[34]See http://www.integratedsoft.com for Integrated Engineering Software IES, COULOMB, AMPERES, and LORENTZ, version 9.0, 2011.
[35]I. Langmuir, "The effect of space charge and residual gases on thermionic currents in high vacuum," Phys. Rev. **2**, 450–486 (1913).
[36]C. D. Child, "Discharge from hot CaO," Phys. Rev. Series I **32**, 492–511 (1911).
[37]F. L. Curzon and B. Ahlborn, "Efficiency of a carnot engine at maximum power output," Am. J. Phys. **43**, 22 (1975).
[38]H. U. Fuchs, *The Dynamics of Heat* (Springer, New York, 1996).
[39]c is not to be confused with the effective concentration c_{eff} that is relevant in the context of PETE. It is $cA_b = c_{eff}A$.
[40]N. D. Lang and W. Kohn, "Theory of metal surfaces: Work function," Phys. Rev. B **3**, 1215–1223 (1971).
[41]W. Shockley and H. J. Queisser, "Detailed balance limit of efficiency of p-n junction solar cells," J. Appl. Phys. **32**, 510–519 (1961).